J. Fluid Mech. (1997), *vol.* 339, *pp.* 199–211

Simulations of the formation of an axisymmetric vortex ring

By R. S. HEEG[1]† AND N. RILEY[2]

[1]Department of Mathematics, University of Groningen, PO Box 800, 9700 AV Groningen, The Netherlands

[2]School of Mathematics, University of East Anglia, Norwich NR4 7TJ, UK

(Received 28 October 1994 and in revised form 2 January 1997)

In this paper we present the results from numerical calculations, based upon the Navier–Stokes equations at relatively high Reynolds number, of the formation of a vortex ring when fluid is ejected from a circular tube. Our results are compared with the experiments of Didden (1979), and the inviscid flow calculations of Nitsche & Krasny (1994). Reasonable agreement is achieved except for the rate of shedding of circulation during the initial stages of ring formation. The theoretically predicted rate of shedding is substantially higher than that predicted by Didden. By contrast the inviscid theory predicts an anomalously high rate of initial shedding. We offer explanations for both of these apparent discrepancies.

1. Introduction

Vortex dynamics is a central theme of fluid dynamics, and a measure of the present interest in it is provided by Saffman's recent monograph (1992). The vortex sheet is a basic model for a free shear layer, and the formation of vortices by rolling up of vortex sheets, which separate at the edge of a body, is a commonly occurring phenomenon in many flow configurations. Such flows in two dimensions, including the initial stages of vortex formation following an impulsive start about a sharp edge, have been extensively studied, see Saffman (1992). Vortex rings have, perhaps, received less attention, although a considerable literature is devoted to them. We are concerned in this paper with the formation, and propagation, of vortex rings when fluid is ejected from a circular nozzle. Our viscous calculations, based upon the Navier–Stokes equations at high Reynolds number, are a complement to the experiments of Didden (1979), and the inviscid model of those experiments by Nitsche & Krasny (1994). Our main aims in the paper are threefold: first to make a comparison with the most detailed experiment of Didden, second to explore the effects of Reynolds number, and finally to offer an explanation for perceived anomalies between theories and between theory and experiment.

In his experiments Didden (1979) created vortex rings by ejecting fluid from a circular nozzle by means of a piston that accelerates from rest to a uniform speed. The vortex sheet that separates at the nozzle edge rolls up to form a vortex ring. This ring propagates axially from the nozzle with its self-induced velocity. The circulation associated with it increases, until the piston motion ceases. By means of laser-Doppler velocimetry Didden has measured the flow properties in the orifice plane, from which

† Present address: Department of Mathematics, University of Twente, PO Box 217, 7500 AE Enschede, The Netherlands.

he has calculated, in particular, the shedding rate of circulation from the orifice lip. In addition he has measured overall flow properties such as ring diameter and speed. Nitsche & Krasny (1994) have constructed an inviscid model of this high-Reynolds-number flow based upon Krasny's vortex-blob method. See, for example, Krasny (1986). The satisfaction of a Kutta condition at the orifice lip determines the shedding rate of circulation . Overall flow properties are fairly well reproduced by the model. These include vortex ring diameter, ring propagation speed and, except in the initial stages of ring formation, circulation shedding rate. Our calculations are based upon the Navier–Stokes equations which we have solved using a finite-difference method, described briefly in §2 below. The calculations are carried out in a finite circular cylindrical container using a non-uniform mesh that allows us to concentrate grid points in the neighbourhood of the orifice lip at which the vortex ring first forms. The piston motion of Didden's experiment is simulated in the nozzle from which the fluid is driven. Our results are presented, and discussed, in §§6, 7 and 8. We can report fairly good overall agreement with Didden's experiments, certainly in respect of ring diameter, propagation speed and, again away from the initial formation phase, circulation shedding rates. Our results provide an indication of the effects of Reynolds number. For example the ring penetration distance during the inflow period increases with Reynolds number, as does the ring diameter. The maximum rate of circulation shedding during ring formation also increases with Reynolds number. The method of Nitsche & Krasny (1994) relies upon a regularizing, or smoothing, parameter δ. In the limit $\delta \to 0$ this will yield a true inviscid, that is infinite-Reynolds-number, solution. The results from their paper that we quote herein are for $\delta = 0.1$. As an inviscid solution their results are consistent with the Reynolds number variations we have described.

The only serious disagreement between, and within, the theoretical and the experimental results lies in the circulation shedding rate during the initial stages of ring formation. Although, as we have indicated, the inviscid results are consistent with our Reynolds number trends, the initial shedding rate of circulation predicted by the inviscid model is anomalously high. It is clear from Nitsche & Krasny's paper that this quantity is initially extremely sensitive to variations in δ. For example the maximum shedding rate drops by 30% as δ changes from 0.2 to 0.1. It would, therefore, appear that in this initial period, of about 0.1 s, the parameter δ is not sufficiently small, and that decreasing it further would yield results that are entirely consistent with our Navier–Stokes calculations. When compared with the experiment of Didden, our Navier–Stokes calculation predicts a circulation shedding rate that is unacceptably high during the piston acceleration phase. However a careful analysis of Didden's results reveals an inconsistency between them that is sufficient to explain the disagreement. We conclude, given the above, that theory at infinite and finite Reynolds numbers, and experiment, are in harmony, and that our calculations at finite Reynolds number not only bridge earlier theoretical and experimental results, but also help to provide an understanding of these interesting and complex flows.

2. Governing equations

2.1. *Equations*

The governing equations are the Navier–Stokes equations for an incompressible fluid. From these we have Helmholtz's equation for the vorticity $\boldsymbol{\omega}'$ as

$$\frac{\partial \boldsymbol{\omega}'}{\partial t'} - \nabla \times (\boldsymbol{v}' \times \boldsymbol{\omega}') = -\nu \nabla \times \boldsymbol{\omega}', \tag{2.1}$$

together with

$$\nabla \cdot \boldsymbol{v}' = 0, \tag{2.2}$$

where ν is the kinematic viscosity, $\boldsymbol{v}'$ is the velocity, t' is time and

$$\boldsymbol{\omega}' = \nabla \times \boldsymbol{v}'. \tag{2.3}$$

In the cylindrical geometry that we work it is convenient to use cylindrical coordinates (r', θ', z') with corresponding velocity components (u', v', w'). In the above equations we make variables dimensionless using a, the radius of the cylinder into which the vortex rings emerge, as a length, U_0 a velocity, and a/U_0 a time, where the typical velocity U_0 is defined below. From the assumptions that the flow is axisymmetric, with no swirl, we have the dimensionless velocity and vorticity given by $\boldsymbol{v} = (u, 0, w)$, $\boldsymbol{\omega} = (0, \zeta, 0)$, where $\zeta = \partial u/\partial z - \partial w/\partial r$. Our computational approach is based upon the stream function–vorticity formulation. We satisfy (2.2) by introducing the stream function ψ such that

$$u = \frac{1}{r}\frac{\partial \psi}{\partial z}, \quad w = -\frac{1}{r}\frac{\partial \psi}{\partial r}. \tag{2.4}$$

Rather than the component of vorticity ζ we choose to work with $\gamma = -r\zeta = r(\partial w/\partial r - \partial u/\partial z)$. The equations satisfied by γ and ψ are then determined from the θ-components of (2.1) and (2.3) as

$$\frac{\partial \gamma}{\partial t} + u\frac{\partial \gamma}{\partial r} + w\frac{\partial \gamma}{\partial z} - \frac{2u\gamma}{r} = \frac{1}{R_a}\left(\frac{\partial^2 \gamma}{\partial r^2} - \frac{1}{r}\frac{\partial \gamma}{\partial r} + \frac{\partial^2 \gamma}{\partial z^2}\right), \tag{2.5}$$

and

$$\frac{\partial^2 \psi}{\partial r^2} - \frac{1}{r}\frac{\partial \psi}{\partial r} + \frac{\partial^2 \psi}{\partial z^2} = -\gamma, \tag{2.6}$$

where $R_a = U_0 a/\nu$ is the Reynolds number that characterizes the flow. We distinguish between this Reynolds number and R_d, the Reynolds number in the experiments of Didden (1979), in §4 below.

2.2. *Computational geometry and boundary conditions*

The computational domain is shown in figure 1. The axis of symmetry lies along $r = 0$, and the nozzle at whose lip the vortex ring forms is defined by $r = r_{ni}$, $0 \leqslant z \leqslant z_n$. The outer surface of the nozzle has $r = r_{no}$. Along $z = 0$, $0 \leqslant r \leqslant r_{ni}$ we impose an inflow condition, and at $z = z_o$, $0 \leqslant r \leqslant 1$ we introduce a suitable outflow condition. The remaining boundaries are impermeable no-slip boundaries.

The boundary conditions to be satisfied at each of these boundaries of the computational domain are as follows. On the axis of symmetry we have

$$\psi = u = \gamma = 0. \tag{2.7}$$

On the impermeable no-slip boundaries we have, for the surfaces $r =$ constant,

$$\psi = c_1(t), \quad w = 0, \quad \gamma = r\frac{\partial w}{\partial r}, \tag{2.8}$$

and for the surfaces $z =$ constant

$$\psi = c_1(t), \quad u = 0, \quad \gamma = -r\frac{\partial u}{\partial r}, \tag{2.9}$$

where c_1 is defined from the inflow conditions. At the inflow boundary we impose a

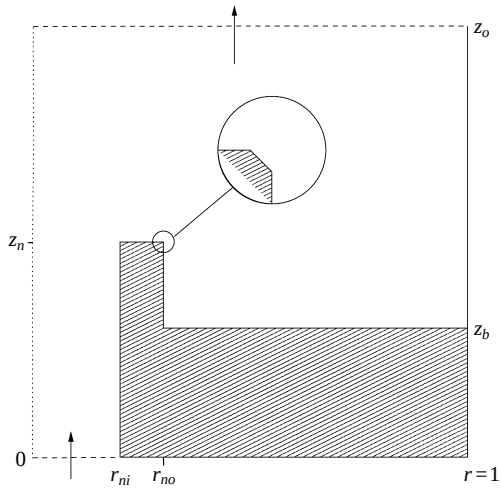

FIGURE 1. Definition sketch. The inset shows the orifice lip shape.

normal velocity $w_0(r,t) = \lambda f(r)g(t)$. The function $g(t)$ represents the motion of the piston which may be accurately determined from the piston trajectory presented by Didden (1979) from the experiment on which we focus our attention. The function $f(r)$ is not so determined, and we subsequently make further assumptions about this quantity. We then have

$$\psi = -\int_0^r s w_0(s,t)\,\mathrm{d}s, \quad w = w_0(r,t), \quad \gamma = r\left(\frac{\partial w_0}{\partial r} - \frac{\partial u}{\partial z}\right), \quad 0 \leqslant r \leqslant r_{ni}, z = 0, \tag{2.10}$$

and $c_1(t) = -\int_0^{r_{ni}} s w_0(s,t)\,\mathrm{d}s$. Finally at the outflow boundary $z = z_0$ we assume conditions are independent of z which will be appropriate if z_0 is sufficiently large. This is implemented by setting

$$\frac{\partial \gamma}{\partial z} = \frac{\partial \psi}{\partial z} = 0, \quad 0 \leqslant r \leqslant 1, \quad z = z_0 - \delta z. \tag{2.11}$$

3. Numerical procedures

The numerical approach is based upon the stream function–vorticity formulation, as represented by equations (2.5) and (2.6). A non-uniform mesh in the (r,z)-plane is used on which all space derivatives are represented by second-order-accurate finite-difference formulae. The time derivative in (2.5) is discretized in the manner of Crank–Nicolson. The representation of the boundary conditions for ψ in finite-difference form is straightforward, as are the conditions on u and w. The conditions on γ in (2.8) and (2.9) at a solid boundary are more complex. It is common practice to follow the method of Woods (1954), using an expansion about the boundary; and this we have done to realize conditions for γ that are second-order accurate. All of the discretized equations and boundary conditions are solved simultaneously at each step, with a Picard-type iteration used to handle the nonlinearity which is implicit in the equations. The equations were solved by the matrix solver BICGSTAB(L) that has been developed by Sleijpen & Fokkema (1993), with a pre-conditioning matrix based on incomplete LU-decomposition as described by van der Ploeg (1992).

The parameters that control the flow under discussion are the Reynolds number R_a (or R_d), and the geometrical parameters. We have used three values of R_d, namely $R_d = 1150, 2300, 4600$. In all the calculations we have set $z_b = 0.5$, $z_n = 0.8$, $z_o = 1.75$, $r_{ni} = 0.2$, $r_{no} = 0.204$. On the scale of Didden's experiments these correspond to $z'_b = 6.25$ cm, $z'_n = 10.0$ cm, $z'_o = 21.875$ cm, $r'_{ni} = 2.5$ cm, $r'_{no} = 2.55$ cm with $a = 12.5$ cm. Although $z'_n - z'_b$ is apparently smaller than in the experiments this is unimportant. For the nozzle itself $(r_{ni} - r_{no})/r_{ni} = 0.02$, exactly as in nozzle 2 of Didden's experiments. We have shaped the nozzle lip itself, as in figure 1, since in practice there will not be an exact right-angled corner.

As we have already remarked, a non-uniform computational mesh is used. This has 159 mesh points in the r-direction, with 295 in the z-direction. In the range $0.1 \leqslant r \leqslant 0.4$, $0.2 \leqslant z \leqslant 1.1$, δr, δz do not exceed $O(10^{-2})$, whilst in the immediate neighbourhood of the lip they are $O(10^{-4})$. In the outer part of the domain they increase to $O(10^{-1})$. Each simulation was started with a time step $\delta t = 10^{-5}$. After a few steps this was increased to 5×10^{-5} and thereafter increased periodically up to $\delta t = 8 \times 10^{-4}$ at $t = 0.4$.

We note at this point that we have tested our solution method, in the absence of a nozzle, in a variety of ways. Thus, we have reproduced exact solutions of the Navier–Stokes equations, we have showns that isolated rings at high Reynolds number propagate according to the asymptotic formula of Saffman (1970), and we have confirmed the solutions of Weidman & Riley (1993) for vortex-ring interactions.

4. The experiment

To complete the formulation of our problem there remains the specification of $w_0(r,t) = \lambda f(r)g(t)$ in (2.10). In the experiments we wish to simulate, Didden (1979) created vortex rings at the lip of the nozzle by driving a piston along it. The piston displacement was accurately measured, and taking the time variation of our input flow at $z = 0$ from the piston trajectory presented by Didden we have (see also Nitsche & Krasny 1994)

$$g(t) = \begin{cases} 0, & t \leqslant 0, \quad t \geqslant t_2, \\ 1 - \left(\dfrac{t_1 - t}{t_1}\right)^{2.8}, & 0 < t \leqslant t_1, \\ 1, & t_1 < t < t_2, \end{cases} \tag{4.1}$$

where $t_1 = U_0 t'_1/a$, $t_2 = U_0 t'_2/a$, with $t'_1 = 0.3$ s, $t'_2 = 1.6$ s in the experiments. Whilst the time variation (4.1) is determined from experiment the form of the radial variation is less obvious. We have taken

$$f(r) = \begin{cases} 1, & r \leqslant r_{ni} - \delta, \\ 1 - \left(\dfrac{r - r_{ni} + \delta}{\delta}\right)^{1.5}, & r_{ni} - \delta < r \leqslant r_{ni}, \end{cases} \tag{4.2}$$

where $\delta = 0.1 r_{ni}(2300/R_d)^{1/2}$ is chosen as a representation of the boundary-layer thickness in the nozzle at $z = 0$, and λ is a parameter that enables us to maintain the same volume inflow rate as in the experiments. In fact the choice for $f(r)$ in (4.2) is not crucial, and not least since fluid particles from $z = 0$ will not reach the lip of the nozzle at time t'_2 in the comparison with the experiment that we make.

We note that Didden bases his Reynolds number upon the nozzle diameter d, so that $R_d = U_0 d/\nu$ and the relationship between R_a and R_d is $R_a = R_d/2r_{ni}$ which cor-

responds, of course, to the relationship between the two length scales $a = d/2r_{ni}$. The characteristic velocity U_0 is taken as the terminal uniform piston speed. The results that Didden presents are for values $U_0 = 4.6$ cm s^{-1}, $U_0 = 6.9$ cm s^{-1}. With a nozzle diameter of 5.0 cm, and water as a working fluid with $\nu = 0.01$ cm^2 s^{-1}, this corresponds to Reynolds numbers $R_d = 2300$, 3450 respectively. The experimental results concentrate almost entirely upon the lower of these Reynolds numbers, in particular the piston trajectory is only given in that case, and it is with these that our comparisons with experiment are made. The effects of varying the Reynolds number are explored by considering the cases $R_d = 1150$, 4600, with $g(t)$, $f(r)$ still as in (4.1), (4.2).

5. Vortex-ring creation: general considerations

Our aim in this investigation is to study the formation, and subsequent behaviour, of a single vortex ring as fluid is forced from a circular orifice, and wherever possible to compare with the experimental results of Didden (1979). In making a comparison with experiment we concentrate upon velocity profiles in the exit plane, the shedding rate of circulation and the trajectory of the vortex rings. Variations with Reynolds number R_d, over a limited range, enable us to place the inviscid results of Nitsche & Krasny (1994), using the vortex blob method, in context.

In our calculations the vortex rings propagate into a circular cylindrical container. By contrast, in the experiments the vortex rings were projected into a tank of square cross-section whose side was almost double the size of our cylinder, and about eight times longer. However the experience of Riley (1993) suggests that the boundaries, radial or axial, will only influence the vortex-ring dynamics when the ring is within a dimensionless distance 0.2 of them. The radial boundary is of particular significance in this respect. A consideration of the image system in $r = 1$ shows that it may be expected to reduce the propagation speed of the vortex rings. In earlier calculations with a uniform mesh, Heeg (1993) made comparisons with $r_n = 0.2$ and $r_n = 0.4$ at Reynolds numbers $R_d = 1150$, 2300. The axial propagation speeds were unchanged, although the ring radii were slightly reduced. With a uniform mesh satisfactory results could not be obtained at higher values of R_d. With the non-uniform grid used in the present calculations the higher resolution that is necessary in the neighbourhood of the nozzle lip, from which the vortex rings are shed, may be achieved. Grid-size checks confirm the accuracy of the results we present up to $R_d = 4600$. Although the results obtained by Heeg (1993) did not allow for a finite nozzle thickness, his results are little different from those presented here.

6. Velocity profiles

In figures 2 and 3 we present axial and radial velocity profiles, for the case $R_d = 2300$, in the nozzle exit plane $z = z_n$ for $r \leqslant r_{ni}$ and $r \geqslant r_{no}$. In these figures we show not only our calculated results but also the experimental results that we have transcribed directly from Didden (1979). Note that we have converted the results of the numerical simulation to dimensional form for comparison with experiment.

The overall features of the experiment are well represented. Within the nozzle, $r < r_{ni}$, the initial phase of developement close to the lip shows an acceleration of the fluid in the boundary layer at the nozzle boundary. This is consistent with an initial potential flow around the lip. As the vortex ring forms this effect dies away, and we have an essentially uniform flow developing at the exit surrounded by a boundary layer on the

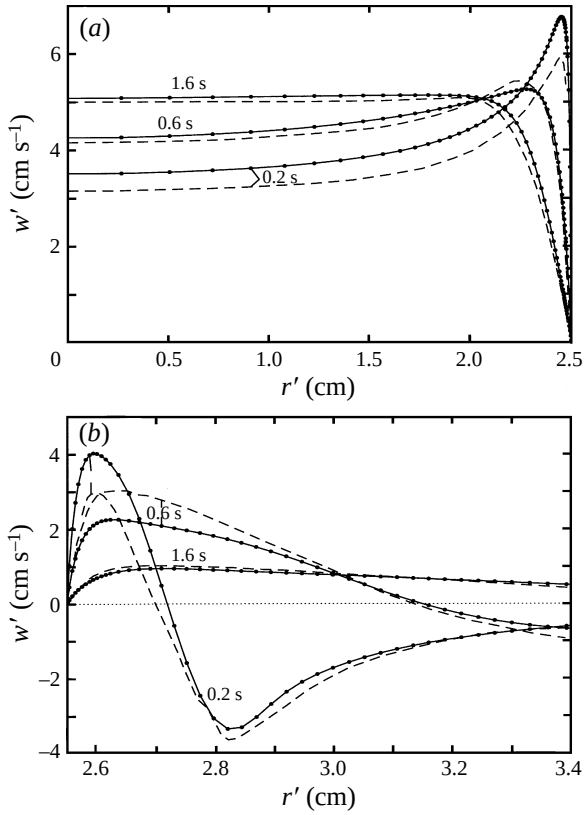

FIGURE 2. Axial velocity profiles in the nozzle exit plane for $R_d = 2300$, calculated results with grid points shown (—●—●—); experiment (– – – –). (*a*) $r < r_{ni}$, (*b*) $r > r_{no}$.

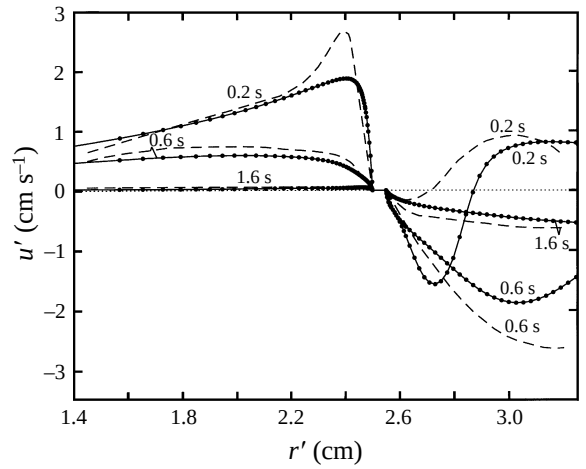

FIGURE 3. As figure 2 but for the radial velocity profiles; for both $r < r_{ni}$, $r > r_{no}$.

wall. For $r > r_{no}$ the axial velocity profiles show features consistent with a neighbouring vortex. Thus, close to the nozzle surface the axial flow is positive, but at a larger radial distance negative. And as the vortex ring propagates away from the nozzle the point of zero axial velocity on $z = z_n$ also moves radially outwards, with the level of the induced axial velocity diminishing. The radial component of velocity in the exit plane is shown in figure 3 for all r. For $r < r_{ni}$ there is flow radially outwards as one may expect. But for $r < r_{no}$ there is flow radially inwards close to the nozzle which is consistent with the presence of the shed vortex ring in $z > z_n$. At $t' = 0.2$ s the vortex lies very close to the exit plane which accounts for the change in sign of velocity at $r' \approx 2.9$ cm.

The agreement between the theoretical and experimental profiles for $r' < 2$ cm and $r' > 3$ cm is reasonable, except at $t' = 0.2$ s, where we see from figure 2(*a*) that within the nozzle there is a persistent and, as we shall see later, significant difference. The explanation for this lies in an apparent inconsistency in Didden's (1979) results. From his figure 2 we see that at $t' = 0.2$ s the piston speed is $0.924U_0$. We can calculate the volume flow rate from this and compare it with the volume flux in the exit plane by using the profile shown in figure 2(*a*). The latter falls short of the required value by 8.5%. Carrying out the same excercise at $t' = 0.3$ s, 1.6 s when the piston speed U_0 is uniform yields differences of -2%, -3% respectively, which are probably within experimental error. As a comparison the flow rates at the exit plane from our computations differ from the known exact value by less than 0.1%, which does add confidence to our results. The inconsistency to which we refer, and which we discuss further in §7 below, is probably due to an inaccurate rendering of the piston trajectory in figure 2 of Didden (1979).

7. Circulation shedding

To calculate the rate of shedding of circulation Γ we may use the result of Didden (1979, 1982), namely

$$\frac{\mathrm{d}\Gamma}{\mathrm{d}t} = \int_0^{r_0} w(r, z_n, t)\zeta(r, z_n, t)\,\mathrm{d}r, \tag{7.1}$$

where r_0 is chosen to lie in the region $\zeta(r, z_n, t) = 0$. In this approach Didden splits the range of integration into $r \leqslant r_{ni}$, $r \geqslant r_{no}$ to calculate separately the circulation shed from the inner and outer surfaces. However, we have found it more convenient to evaluate $\mathrm{d}\Gamma/\mathrm{d}t$ at each instant of time from

$$\Gamma(t) = \int_S \zeta(r, z, t)\,\mathrm{d}z\,\mathrm{d}r, \tag{7.2}$$

where the domain of integration S is that part of our computational domain with $z > z_n$, and $r < 0.9$ which specifically excludes any vorticity created at the outer boundary. This assumes that the total vorticity shed lies in $z > z_n$ and does not penetrate the outer boundary layer at $r = 1$.

We have evaluated $\mathrm{d}\Gamma/\mathrm{d}t$ for each of the Reynolds numbers $R_d = 1150$, 2300, 4600 and the results are shown in figure 4. We also include in this figure the circulation shedding rate estimated by Didden from his experiment with $R_d = 2300$ and also that calculated by Nitsche & Krasny (1994) from their inviscid vortex-blob method. The results in figure 4 are again presented in dimensional form.

Consider first the results obtained from our simulations. In all three cases the shedding rate increases and reaches a maximum at $t' = 0.2$ s, with the maximum shedding rate increasing with R_d. This rise in shedding rate during the first fraction of a second may be attributed to the velocity field of accumulating vorticity at the nozzle lip, as

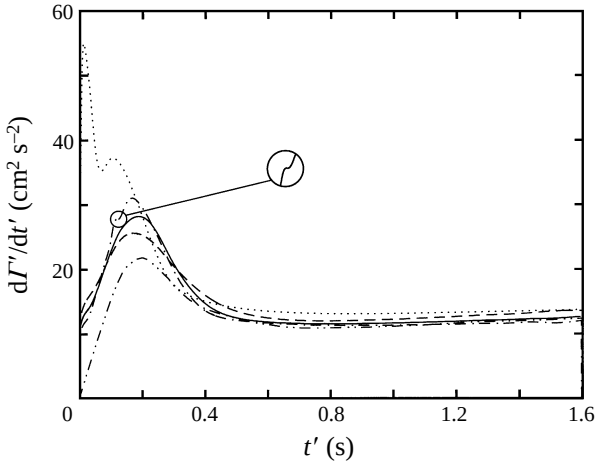

FIGURE 4. The shedding rate of circulation. Simulation at $R_d = 2300$ (—), experiment (-·-·-), inviscid result of Nitsche & Krasny (1994) (·····), simulation at $R_d = 1150$ (----), simulation at $R_d = 4600$ (-·-·-).

noted in figure 2. Subsequently the self-induced velocity moves this vorticity, as a ring, away from the nozzle. During this phase the shedding rate falls until the ring itself makes no contribution to it and, in each case, it assumes an almost constant value for $t' \geqslant 0.6$ s, with little Reynolds number variation, until the inflow ceases. Didden's experimental result with $R_d = 2300$ shows similar features, but during the initial period of piston acceleration the shedding rate falls consistently below the simulation at the same Reynolds number. In discussing the velocity profiles in §6 above we have identified an inconsistency within Didden's results. This now clearly manifests itself in the circulation shedding rate which is lower than implied by the piston trajectory shown in figure 2 of Didden (1979). The present simulation and the experiment are therefore not necessarily inconsistent. Consider next the inviscid result of Nitsche & Krasny (1994) shown in figure 4. Their vortex-blob method involves the use of a parameter, δ, to regularize the roll-up of the free vortex sheet consequent upon the application of a Kutta condition at the orifice lip. In their paper results are presented for values of $\delta = 0.1, 0.2, 0.4$. The result shown in figure 4 corresponds to $\delta = 0.1$. The vortex-blob method is expected to yield an inviscid solution in the limit $\delta \to 0$. The most striking feature of the inviscid result in figure 4 is the sharp peak at $t'_s \approx 0.015$ s. However this is strongly dependent upon δ, and indeed only 70% of the peak value at $\delta = 0.2$. Decreasing δ further can be expected to lead to a further reduction in this peak. It may also be noted that in the simulation for $R_d = 4600$ there is a development at $t' \approx 0.1$ s which appears to be forming a local maximum. As a consequence we believe that the inviscid result and high-Reynolds-number simulation are not inconsistent; indeed we consider that our results provide powerful support in favour of the vortex-blob method for inviscid flow, for which the present problem is a severe test.

In figure 5 we show the variation with time of the total shed circulation. This proves to be relatively insensitive to Reynolds number variations. During the initial formation period it increases slightly with Reynolds number, whilst at the point $t' = 1.6$ s, when inflow ceases the reverse is the case. The experimental value falls short of the calculated value at $R_d = 2300$ by about 10% which is due to the lower shedding rate in the initial stages as we have already discussed. The inviscid result is somewhat higher than might be expected in the limit $R_d \to \infty$ due to an overestimate

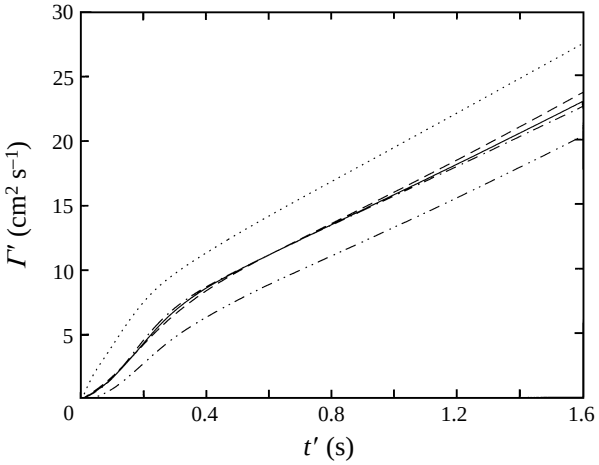

FIGURE 5. The total shed circulation. Simulation at $R_d = 2300$ (—), experiment (-·-·-), inviscid result of Nitsche & Krasny (1994) (·····), simulation at $R_d = 1150$ (----), simulation at $R_d = 4600$ (-·-·-).

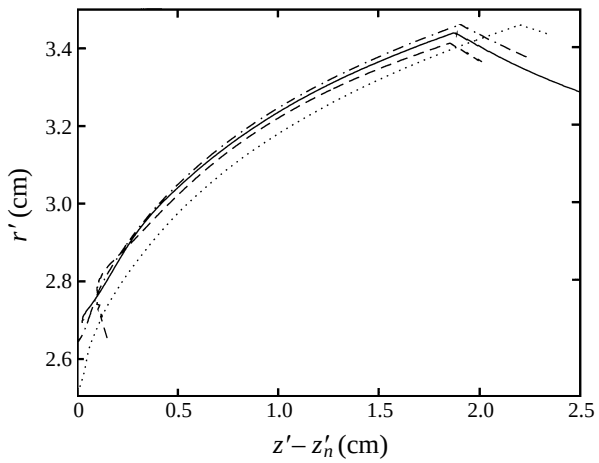

FIGURE 6. The vortex ring trajectories. Simulation at $R_d = 2300$ (—), inviscid result of Nitsche & Krasny (1994) (·····), simulation at $R_d = 1150$ (----), simulation at $R_d = 4600$ (-·-·-).

of the shedding rate by the vortex-blob method. This is most apparent in the early stages, but is not insignificant at the end of the inflow period, as may be noted from figure 12(*c*) of Nitsche & Krasny (1994).

8. Vortex-ring trajectories

The trajectory $r = r_t(z)$ of the vortex rings has been measured in the experiments and estimated from both the numerical simulations in our finite-Reynolds-number calculations and in the inviscid calculations of Nitsche & Krasny. The theoretical estimate of the vortex-ring position uses, in all cases, the point of maximum vorticity rather than the centroid of the vorticity distribution in a cross-section of the ring. But at high Reynolds number we may expect these to be almost coincident. In figure 6 we compare the theoretical trajectories at different Reynolds numbers, whilst in figure 7

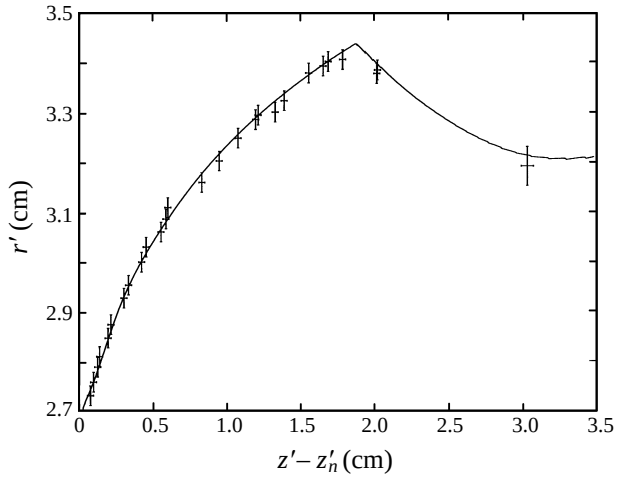

FIGURE 7. A comparison between the theoretical and experimental vortex trajectories at $R_d = 2300$. Simulation at $R_d = 2300$ (—), experiment (+).

we make a comparison between our present results and experiment at $R_d = 2300$. The results are again presented in dimensional form.

Consider first figure 6. In all the cases considered the vortex rings increase in diameter until the inflow ceases. Thereafter there is an abrupt contraction of the ring. Didden suggests that this is largely due to the influence of the nozzle boundary. However, when the inflow ceases a secondary vortex ring is observed to form at the tube exit and a referee has made the suggestion, with which we concur, that its presence results in the contraction. The Reynolds number dependence that may be inferred from the point of inflow cessation is that as R_d increases the ring diameter increases as does the speed of the vortex ring. We also include in figure 6 the inviscid result of Nitsche & Krasny for $\delta = 0.1$ which, as we expect, yields a faster-moving ring. However from results they present, which again show a strong dependence on δ, we infer that the limiting solution for $R_d \to \infty$, that is as $\delta \to 0$, will yield a slower-moving ring with larger diameter than shown in figure 6, consistent with the trends we have established at large, but finite, Reynolds number. In figure 7 we compare the theoretical and experimental trajectories at $R_d = 2300$. Judged again from the results at inflow cessation, the ring is predicted to have a slightly larger diameter and higher speed. This is consistent with the shortfall in shed vorticity discussed above; otherwise the agreement is good.

It has been noted by both Didden (1979) and Nitsche & Krasny (1994) that in the early stages of ring formation the solution does not conform to the similarity result of Pullin (1979). If r_c, z_c denote the coordinates of the vortex position measured from the tube edge, then we would expect $r_c \sim t^{2/3}$, $z_c \sim t^{2/3}$. However, whilst r_c behaves reasonably well in this manner, both Didden and Nitsche & Krasny find that z_c is more accurately represented by $z_c \sim t^{3/2}$. Our results confirm this as may be seen in figure 8. In this figure we use, just as Nitsche & Krasny (1994), the shifted time $t_* = t' - t_{eff}$, where $t_{eff} = 0.078$ is the effective time origin defined by

$$\int_0^{t'} g(t)\,\mathrm{d}t = t' - t_{eff}. \tag{8.1}$$

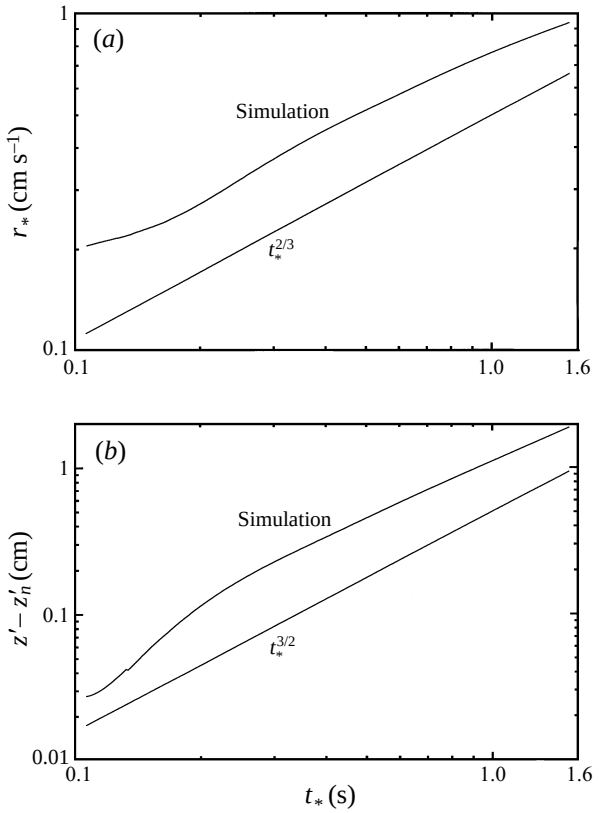

FIGURE 8. Logarithmic plots of the vortex position measured from the tube edge, time $t_* = t' - t_{eff}$. (*a*) Radial coordinate, $r_* = r_c - r_{ni}$, (*b*) axial coordinate.

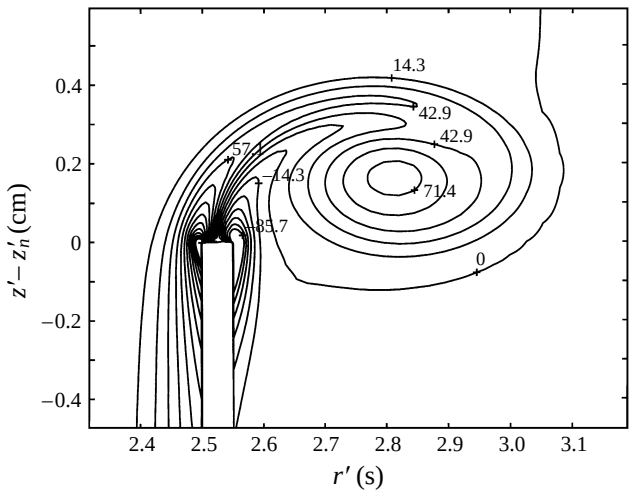

FIGURE 9. A vorticity contour plot at $t' = 0.32$ s for the case $R_d = 2300$.

The reasons for this discrepancy have not been clear, but we offer the following suggestions. Certainly during the period of inflow acceleration, up to $t' = 0.3$ s, the flow cannot be expected to be of similarity form. In figure 9 we show a section of the ring just beyond that time, at $t' = 0.32$ s chosen to coincide with a time at which Didden and Nitsche & Krasny present flow visualizations (for a range of such visualizations from both experiment and inviscid theory see figure 4 of Nitsche & Krasny 1994). The similarity theory is based upon the notion that the vortex ring grows within a known potential flow. However the scale of the vortex for times $t' > 0.3$ s suggest that such a notion may not be appropriate. Nitsche & Krasny also draw attention to the effect of the ring's self-induced velocity upon the similarity theory. On these bases it seems reasonable to propose that the similarity theory may only apply for very short times, typically up to the time of maximum shedding rate of vorticity. In the present case that would be $t' = 0.2$ s, which is not in the time range the similarity theory can be expected to apply anyway.

The authors are indebted to Arthur Veldman and Monika Nitsche for valuable discussions. Also to Auke van der Ploeg for providing us with his implementation of the matrix solver and preconditioner we have used. Furthermore R.S.H. acknowledges the financial support of the Rijksuniversiteit Groningen which enabled him to visit the University of East Anglia, where most of the preparations for the calculations described herein were carried out. And last, but not least, R.S.H. thanks the University of Enschede for providing computing time for the computations which were used in this revised version.

REFERENCES

Didden, N. 1979 On the formation of vortex rings: rolling-up and production of circulation. *J. Appl. Math. Phys.* **30**, 101–116.

Didden, N. 1982 On vortex-ring formation and interaction with solid boundaries. In *Vortex Motion* (ed. H. G. Hornung & E.-A. Müller). Friedr. Vieweg and Sohn.

Heeg, R. S. 1993 Simulations of the creation and motion of vortex rings. *Rep.* W-9319. University of Groningen.

Krasny, R. 1986 Desingularization of periodic vortex sheet roll-up. *J. Comput. Phys.* **65**, 292–301.

Nitsche, M. & Krasny, R. 1994 A numerical study of vortex ring formation at the edge of a circular tube. *J. Fluid Mech.* **276**, 139–161.

Ploeg, A. van der 1992 Preconditioning techniques for non-symmetric matrices with application to temperature calculations of cooled concrete. *Intl J. Numer. Meth. Engng* **35**, 1311–1328.

Pullin, D. I. 1979 Vortex ring formation at tube and orifice openings. *Phys. Fluids* **22**, 401–403.

Riley, N. 1993 On the behaviour of pairs of vortex rings. *Q. J. Mech. Appl. Maths* **46**, 521–539.

Saffman, P. G. 1970 The velocity of viscous vortex rings. *Stud. Appl. Maths* **49,** 371–380.

Saffman, P. G. 1992 *Vortex Dynamics.* Cambridge University Press.

Sleijpen, G. L. G. & Fokkema, D. R. 1993 BICGSTAB(L) for linear equations involving unsymmetric matrices with complex spectrum. *Elect. Trans. Numer. Anal.* **1,** 11–32.

Weidman, P. D. & Riley, N. 1993 Vortex-ring pairs: numerical simulation and experiment. *J. Fluid Mech.* **257**, 311–337.

Woods, L. C. 1954 A note on the numerical solution of fourth-order differential equations. *Aero. Q.* **5,** 177–182.